

Article

Development of a Robotic Arm Based Hydrogel Additive Manufacturing System for In-Situ Printing

Xiao Li ^{1,2,3}, Qin Lian ^{1,2,3,*}, Dichen Li ^{1,2,3}, Hua Xin ¹ and Shuhai Jia ¹

¹ State Key Laboratory for Manufacturing System Engineering, Xi'an Jiaotong University, Xi'an 710054, China; lx2811161@163.com (X.L.); dcli@mail.xjtu.edu.cn (D.L.); HuaXin2015@xjtu.edu.cn (H.X.); shjia@mail.xjtu.edu.cn (S.J.)

² Rapid Manufacturing National Engineering Research Center, Xi'an Jiaotong University, Xi'an 710054, China

³ The High-end Manufacturing Equipment Collaborative Innovation Research Center, Xi'an Jiaotong University, Xi'an 710054, China

* Correspondence: lqiamt@mail.xjtu.edu.cn; Tel.: +86-29-8339-5187

Academic Editor: Peter Van Puyvelde

Received: 24 November 2016; Accepted: 9 January 2017; Published: 11 January 2017

Abstract: In-situ printing is a promising injury repair technique that can be directly applied during surgical operations. This paper features a potential in-situ printing platform based on a small-scale robotic arm with a micro-sized dispenser valve. A double-light-source curing method was applied to print poly(ethylene glycol) diacrylate (PEGDA) with a 20% (weight/volume) ratio and the entire process was controlled automatically by a computer interface where droplet diameter, curing time, mechanical properties were measured and essential printing parameters (e.g., nozzle velocity, nozzle frequency) were determined. Three different two-dimensional (2D) plane models (namely, square, circular, and heart-shaped) were printed during initial printing trials. The feasibility study of in-situ printing on curved surfaces was tested using a three-dimensional (3D) printed defect model. The defect was successfully filled using both parallel and ring printing paths. In conclusion, the robotic arm printing platform and its forming method can achieve a rapid curing of PEGDA hydrogel on a curved surface and has the potential to be applied to in-situ printing.

Keywords: in-situ printing; robotic arm; double-light-sources curing; inkjet printing; poly(ethylene glycol) diacrylate (PEGDA) hydrogel

1. Introduction

In-situ printing is a state-of-the-art technique which can directly repair the defect site according to its geometric features [1,2]. Compared to common three-dimensional (3D) printing, also known as additive manufacturing (AM), in-situ printing is more applicable to injury repair due to the fact that the defects normally involve curved surfaces or even more complex geometry, while 3D printing is limited to a flat substrate. Thus far, studies on in-situ printing have focused on the repair of skin and cartilage [1].

Researchers at Wake Forest University have repaired the skin defect (full thickness) on the back of a nude mouse using in-situ printing. A micro-valve is used to print fibrin and collagen mixed with fibroblasts and keratinocytes along the curved surface (one drop per millimeter) [3]. One issue with this method is that the curing time for thrombin and collagen is normally longer than 15 min and that possible material flow may occur during curved surface in-situ printing due to the fact that the printed liquid is not cured in time.

A bio-printing system developed by the Scripps Research Institute is suitable for cartilage in-situ repairing. A modified HP 500 inkjet printer is used to print poly(ethylene glycol) dimethacrylate (PEGDMA) with human chondrocytes. Results show the osteochondral defect is successfully repaired

layer by layer. The printed cartilage is firmly attached to the surrounding tissues and proteoglycan deposition is observed [4]. However, repairing the cartilage in this way does not involve curved surface forming, whereas in actual tissue repair, curved surface forming is unavoidable. Other studies on in-situ cartilage repair, using injection [5] or pouring [6] methods to fill the defects, demonstrate uncertain forming precision due to their manual operation.

The development of in-situ printing technology makes it feasible to directly fill defects and repair tissue during surgical operations. A flexible and precise position control system is essential for in-situ printing. A versatile robotic arm (e.g., Leonardo Da Vinci surgical robots) is a possible solution which occupies little operating-room space and can perform a variety of surgical procedures [7]. A robotically controlled additive manufacturing system has been developed by Massachusetts Institute of Technology using Kuka Agilus KR1100. The working space is 1000 mm × 500 mm, and large-scaled biodegradable composite is produced using chitosan and sodium alginate [8]. However, the synchronous control of robotic movement and extrusion nozzle is not achieved.

Hydrogel with a large amount of water and a cross-linked network structure is widely used in the study of tissue engineering [9,10]. The curing time and forming control of hydrogel present difficulties in the manufacturing of biological scaffolds [11]. Light curing technology is one of the most widely used methods for 3D printing, and it is widely used in biological printing [12]. In our previous studies, a single-light-source curing method was applied [13]. However, due to the uneven distribution of light intensity, the formed hydrogel structures showed poor geometric accuracy. To solve this problem a symmetrical light source with more uniform light intensity is applied to replace the single light source.

In this study, a brand new in-situ printing platform was set up and the feasibility study of in-situ printing was carried out. A small-scale robotic arm was used as the motion system. A special inkjet printing nozzle system was custom designed. PEGDA light curable biological hydrogel was used as the bio-material. Essential printing parameters were determined and the in-situ curved surface forming process was studied.

2. Robotic Arm Printing Platform

2.1. Hardware

The robotic arm printing platform (as shown in Figure 1) consists of a robotic arm (Dobot version 1.0, Shenzhen Yuejiang Technology Co., Ltd., Shenzhen, China), an Arduino singlechip (UNO R3, Shanghai Langyi Electronics Technology Co., Ltd., Shanghai, China), a leeco micro-valve (INKX0514300A, Lee Company, Westbrook, CT, USA), a light source (UVXON, Shenzhen Youxi Technology Co., Ltd., Shenzhen, China), a relay, a computer and feeding equipments.

In Figure 1a, the computer is connected to the Dobot controller (Shenzhen Yuejiang Technology Co., Ltd., Shenzhen, China) and Arduino singlechip via the USB interface. Arduino singlechip is connected to the light source controller (Shenzhen Youxi Technology Co., Ltd., Shenzhen, China) and nozzle controller (Lee Company, Westbrook, CT, USA). The relay is used to connect the Arduino singlechip and the light source controller.

The robotic arm is composed of a base, a rear arm, a fore arm and an end-effector. It has three degrees of freedom and is driven by three stepper motors. The angles of the robotic arm are measured by the sensors SCA1000-D01 (Shenzhen Yuejiang Technology Co., Ltd., Shenzhen, China) mounted on the rear arm and fore arm. The end-effector can move within a circle with a radius of 320 mm and the positioning accuracy is ± 0.1 mm.

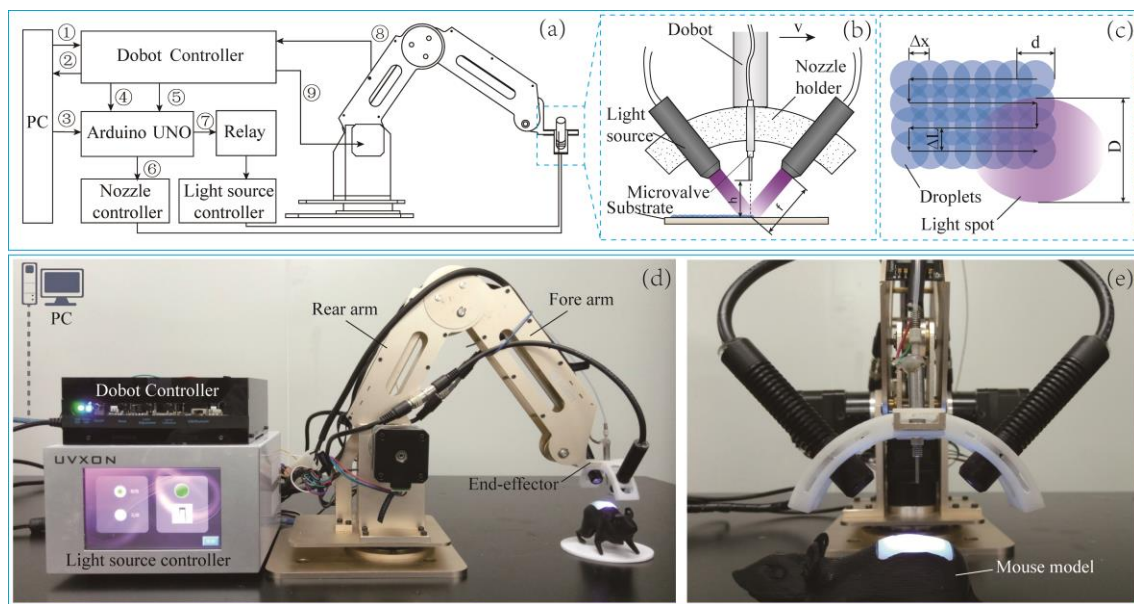


Figure 1. (a) Schematic diagram of hardware structure (① computer control signal, ② robotic arm feedback signal, ③ nozzle frequency signal, ④ synchronously control signal, ⑤ separately controlled signal, ⑥ nozzle switch signal, ⑦ light sources switch signal, ⑧ angle signal, ⑨ stepper motor control signal); (b) schematic diagram of nozzle structure; (c) top view of printing process; (d) robotic arm printing platform; (e) double-light-source inkjet light curing nozzle.

2.2. Nozzle

A double-light-source inkjet light-curing nozzle system is custom designed and consists of a micro-valve, two ultraviolet (UV) light sources (symmetrical arrangement) and a nozzle holder (as shown in Figure 1b,e). The micro-valve and two light sources are mounted onto the nozzle holder; the distance between nozzle and substrate is 15 mm (h). Material is pressed into the nozzle from a nozzle tail pipe with a pressure of 0.05 MPa. The nozzle is 0.1 mm in diameter and 10 nanoliters of material can be ejected per drop.

In Figure 1b, the wavelength of UV light is fixed at 365 nm, the focal length is 20 mm (f), the light spot diameter (D) is 6 mm and the incident angle is 45° . The energy power of the double light source is 267 mW and the average energy density is 940 mW/cm^2 .

As shown in Figure 1c, the droplets are ejected from the nozzle at the frequency F to form a continuous line with the movement of the nozzle. The UV light spot is just below the nozzle to cure the ejected material. It is assumed that the time required for the ejected material to be cured completely is t . The velocity of the nozzle (v) is denoted as Equation (1). Where D is the light spot diameter, d is the droplet diameter:

$$v = \frac{D - d}{2t} \tag{1}$$

Nozzle frequency (F) is related to the nozzle velocity (v) and the droplet spacing (Δx), as shown in Equation (2).

$$F = \frac{v}{\Delta x} \tag{2}$$

The droplet diameter (d), curing time (t), droplet spacing (Δx), line spacing (ΔL) should be determined before printing.

2.3. Software

Software is cooperating with the hardware during the entire printing process. The operation interface (as shown in Figure 2) and functions of the robotic arm printing platform are written

with Qt Creator 5.5.1 (Qt Company, Espoo, Finland). These functions include motion control (i.e., manual calibration operation and playback operation) as well as nozzle and light source control (i.e., independent control and coordinated control). The communication between computer and the robotic arm is through the serial port. The communication protocol adopts a fixed frame format with 42 bytes per frame.

The program of Arduino singlechip is written with Arduino IDE 1.6.7 (Arduino.cc, Turin, Italy). It includes reading the nozzle and light sources control signal, sending a certain frequency of 0–5 V gate signal to the nozzle controller and sending switch signal to light source controller. The singlechip is a bridge to realize synchronous control of the robotic arm and the nozzle.

File conversion software is written with Qt Creator 5.5.1 in order to convert the G code file which contains the absolute coordinate information to an Extensible Markup Language (XML) file which contains the relative coordinate information, nozzle switch information, and movement speed information (all software codes are in Supplementary Materials).

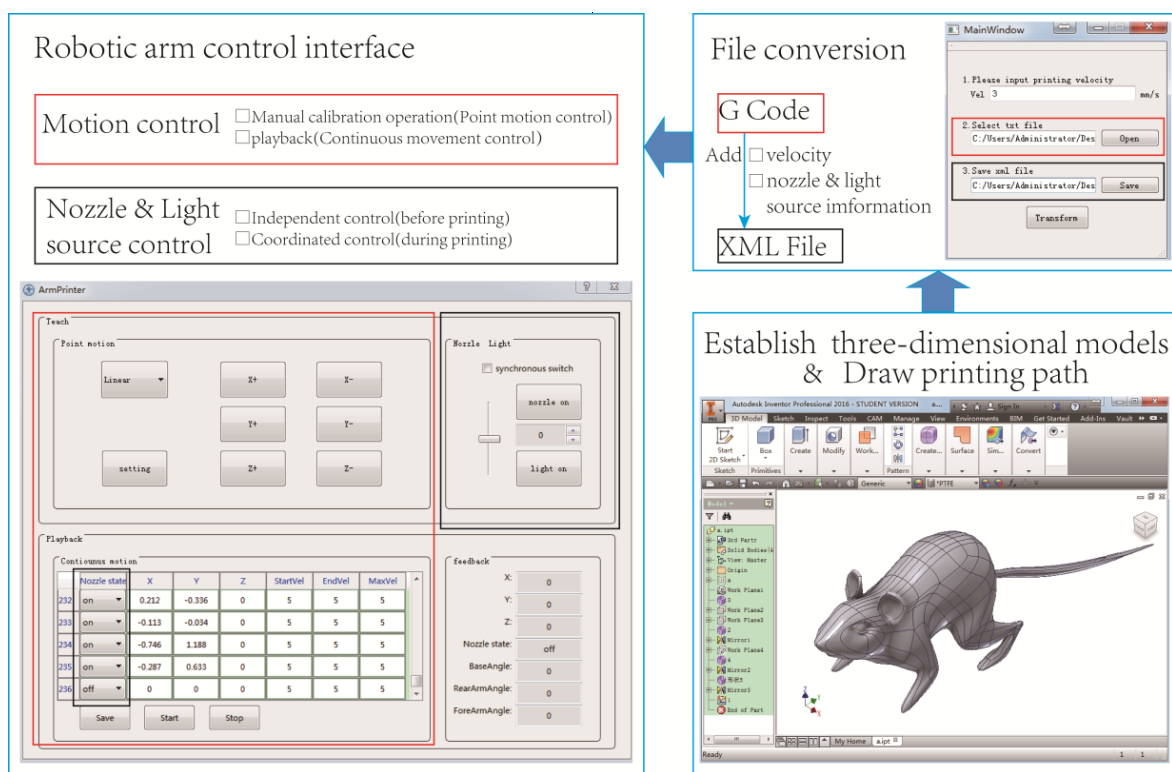


Figure 2. Model building, file conversion and robotic arm control interface.

3. Forming Process

3.1. Materials

Poly(ethylene glycol) diacrylate (PEGDA, Mn = 1000) was obtained from Aladdin, Shanghai, China. Irgacure 2959 was obtained from Sigma-Aldrich Company, St. Louis, USA. PEGDA and Irgacure 2959 were mixed together using deionized water (Sichuan excellent water treatment equipment Co., Ltd., Chengdu, China). A series of solutions were obtained with different PEGDA concentrations (15%, 20%, 25%, 30%, 35% w/v), and the Irgacure concentration stayed the same 0.5% (w/v). Stir mixing was performed for at least half an hour in order to achieve complete dissociation of the solute.

3.2. Methods

3.2.1. Measurement of Droplet Diameter

Droplet diameter is related to the printing parameters. Because there is overlap between adjacent droplets in the printing process (as shown in Figure 1c), the investigation into whether overlapping droplets affect the droplet diameter should be conducted. Single droplet (no overlap) and double droplets (two drops of material were continuously printed in the same position resulting in 100% overlap) of 20% (*w/v*) PEGDA were printed by the nozzle system on the substrate respectively, and the diameter of the droplets was measured using an inverted fluorescence microscope (Ti-s, Nikon, Tokyo, Japan). Six samples were measured for each group; mean value and standard deviation were calculated.

3.2.2. Measurement of Curing Time

Curing time of material is a vital parameter for rapid prototyping. In order to ensure that the material can be completely cured in a certain time, double droplets of 20% (*w/v*) PEGDA and different illumination time lengths were used to measure the curing ratio. After illumination, the uncured liquid was blotted up by absorbent paper. The diameter of the droplets before and after illumination was measured using an inverted fluorescence microscope. The ratio of droplet diameter after and before curing was defined as the curing ratio. The time of illumination was 0.2, 0.3, 0.4, 0.5, 0.6, 0.7, and 0.8 s; three samples were measured for each time length; mean value and standard deviation were calculated.

3.2.3. Initial Printing Trials

In order to verify the functions of the robotic arm printing platform and test the feasibility of parameters in practice, square, circular, and heart-shaped two-dimensional (2D) plane models were created by Inventor software (Professional 2016, Autodesk, Inc., San Rafael, CA, USA). The printing paths were generated by Inventor HSM software (Professional 2016, Autodesk, Inc., San Rafael, CA, USA). A thickness monitor with a precision of 0.001 mm (Mitutoyo, Kawasaki, Japan) was used to measure the thickness of the single layer of the formed hydrogel. Three samples were printed for each shape and each sample was measured three times; mean value and standard deviation were calculated.

3.2.4. Mechanical Testing

The compressive tests were conducted on PEGDA hydrogels with varied weight/volume concentration using a universal mechanical testing machine (103A, Shenzhen Wance Test Equipment Co., Ltd, Shenzhen, China). The test samples were cylinders with a diameter of 6.3 mm and a height of 3 mm. 15%, 20%, 25%, 30%, and 35% (*w/v*) of PEGDA concentrations were poured into the mold respectively, and illuminated for 15 s to cure completely. The compression rate was set at 0.25 mm/min and the test was finished once the strain reached to 15%. The stress-strain curves were obtained; the elastic modulus was calculated using the strain range from 5% to 10%. Six samples were measured in each group; mean value and standard deviation were calculated.

3.2.5. In-situ Printing Experiment

In Figure 3, an in-situ printing experiment was performed on a model with a 15 mm × 10 mm × 1 mm skin defect. The position of the skin defect was fixed during the in-situ printing and the nozzle was adjusted by the manual calibration operation to the start position. The defect model was made by SLA 3D printing. In order to be more realistic, it could be in a mouse model. Ring and parallel paths were generated. The other parameters such as starting position and precision of the paths were pre-defined. Two layers of hydrogel were printed on the defect site.

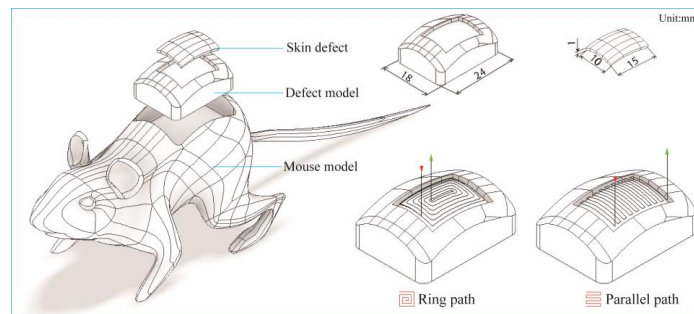


Figure 3. Defect model and skin defect with dimensions and in-situ printing paths; defect model could be embedded in the mouse model.

3.3. Results

3.3.1. Droplet Diameter

Table 1 shows the droplet diameter of single and double droplets. The diameter of a single droplet was 1.306 ± 0.052 mm and double droplets was 1.483 ± 0.027 mm. The number of droplets doubled while the droplet diameter increased only $13.6\% \pm 7.1\%$ (calculated according to the error transfer formula). Droplet overlap had a slight effect on droplet diameter, so that the diameter of a single droplet was adopted as droplet diameter (d) in the following experiments.

Table 1. The measured droplet diameters of single droplet and double droplets. Mean value \pm standard deviation.

Number	Droplet Diameter/mm	
	Single Droplet	Double Droplets
1	1.273	1.505
2	1.362	1.458
3	1.351	1.496
4	1.340	1.444
5	1.278	1.483
6	1.234	1.511
Mean \pm SD	1.306 ± 0.052	1.483 ± 0.027

3.3.2. Curing Time

The calculated curing ratio was plotted against the illumination time in Figure 4. PEGDA liquid began to cure after 0.2 s of illumination. The droplet was gradually cured as the illumination time extended. Complete curing was achieved after 0.8 s of illumination.

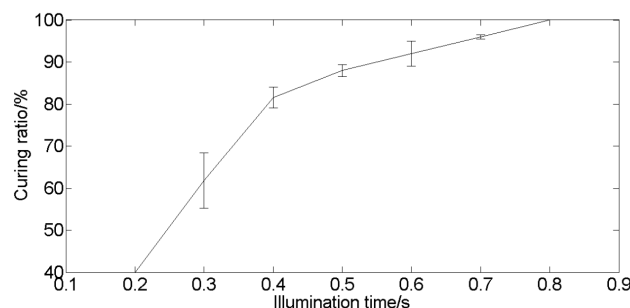


Figure 4. The relationship between curing ratio and illumination time. The data points were linked together by straight line. Error bars represent the standard deviation. Three samples were taken for each illumination time.

3.3.3. Initial Printing Trials

Initial printing trials were performed to print 2D structures using the parameters listed in Table 2. In order to form a smooth line, both droplet spacing (Δx) and line spacing (ΔL) were set as 0.75 mm so that about half of the two droplets could overlap together. The nozzle velocity (v) and nozzle frequency (F) were calculated according to Equations (1) and (2). Three different plane shapes were printed using PEGDA hydrogel (as shown in Figure 5). In visual observation, the formed hydrogel structures were transparent with adequate water content. The outer contour was intact with a smooth appearance. The thickness of formed hydrogel was $466 \pm 6 \mu\text{m}$ (square), $471 \pm 5 \mu\text{m}$ (circular) and $470 \pm 7 \mu\text{m}$ (heart-shaped). The thickness was independent of the geometrical shapes.

Table 2. Printing parameters of initial printing trials.

Parameter	Value	Unit
Droplet diameter d	1.3	mm
Light spot diameter D	6.0	mm
Curing time t	0.8	s
Droplet spacing Δx	0.75	mm
Line spacing ΔL	0.75	mm
Nozzle velocity v	3.0	mm/s
Nozzle frequency F	4.0	Hz

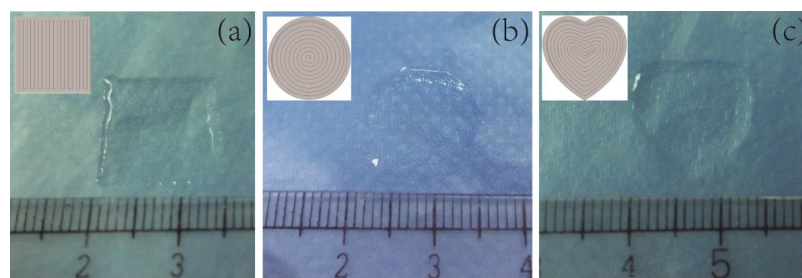


Figure 5. (a) Square printing results; (b) circular printing results; (c) heart-shaped printing results. The printing path is in the upper left corner of each picture.

3.3.4. Mechanical Testing

The obtained elastic modulus had a linear proportion to the PEGDA concentration (as shown in Figure 6). The elastic modulus of 15% PEGDA was $0.266 \pm 0.006 \text{ MPa}$. In contrast, the elastic modulus of 35% PEGDA was $2.495 \pm 0.011 \text{ MPa}$. The elastic modulus of the 20% PEGDA we used was $0.770 \pm 0.006 \text{ MPa}$.

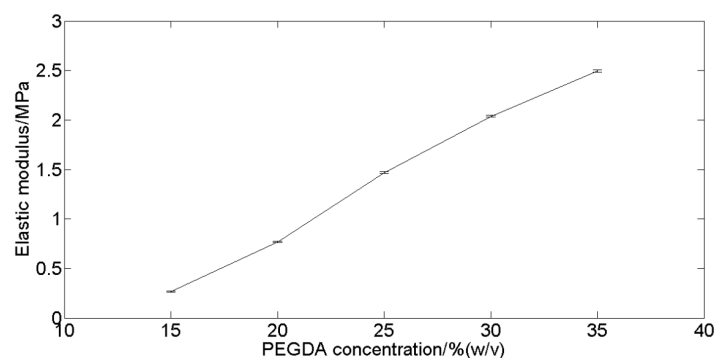


Figure 6. The relationship between elastic modulus and poly(ethylene glycol) diacrylate (PEGDA) concentration. The data points were linked together by straight line. Error bars represent the standard deviation. Six samples were taken for each concentration.

3.3.5. In-Situ Printing

The feasibility study of in-situ printing was carried out using the parameters listed in Table 2. Pictures of in-situ printing outcomes were shown in Figure 7. Both printing paths were capable to fill the defect site completely. It can be seen by visual observation that the material was cured completely and no bubbles or cracks were found. The cured PEGDA hydrogel surface had a certain curvature and the difference between the results of two kinds of printing paths was not obvious.

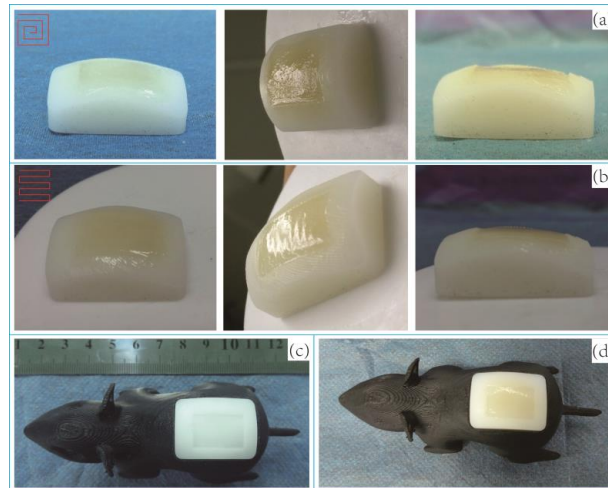


Figure 7. (a) The defect was filled by ring path in-situ printing; (b) the defect was filled by parallel path in-situ printing; (c) mouse model with unfilled defect; (d) mouse model with filled defect.

4. Discussion

Compared to traditional 3D printing platforms, a robotic arm has a more open printing space. In previous studies [8], robotic movement and extrusion are not explicitly linked, thereby the robotic arm and extrusion nozzle can only be controlled independently. In this paper, the motion of the robotic arm and the control of the nozzle and light sources were integrated together; the entire printing process was under synchronous control using the same computer operation interface. Therefore, the automation degree of the equipment was improved and in-situ printing was more convenient.

Material flow is a critical concern for in-situ printing on large-scaled curved surfaces and the forming accuracy is normally affected. Light-curing illumination can be employed either after deposition of material or during the printing process, and the latter is more conducive to achieve a rapid curing [14]. In order to ensure a rapid solidification of liquid material, a double-light-source nozzle system was applied. Because the droplet size was small and had a relatively high energy density, the actual curing time could be reduced down to 0.8 s. Moreover, the symmetrical arrangement of light sources ensured the uniformity of light density so that the base material was evenly cured on both sides instead of on one side when using the single light source. The geometric accuracy of formed structures was therefore improved.

Polyethylene glycol (PEG) is one of the most widely used synthetic materials because of its hydrophobicity, biocompatibility, and because it is easy to modify. PEGDA is synthesized from PEG by diacrylate modification, which is a hydrogel precursor. After the addition of the photo initiator, the light curing reaction can occur by irradiation of UV light [15,16]. In mechanical testing, a monotonic positive relationship was observed. It is obvious that the mechanical property of the hydrogel is governed by the PEGDA solute. A higher PEGDA concentration leads to a higher elastic modulus. This phenomenon means that the mechanical properties of PEGDA hydrogel can be tailored to match versatile application requirements. For instance, a low mechanical strength hydrogel can be used to repair skin while a relatively high mechanical strength hydrogel can repair cartilage [17].

In this paper, a 20% (*w/v*) PEGDA solution was chosen as the printing concentration, because this concentration has the appropriate formability and mechanical properties. Cornell University uses 20% (*w/v*) PEGDA as biomaterial to optimize the parameters of a bio-printer [18]. The Illinois Institute of Technology chooses 15%, 25%, and 40% (*w/v*) PEGDA as the material to analyze cell adhesion and proliferation. The results show that increases in hydrogel concentration cause decreases in cell adhesion and increases in proliferation [19]. Therefore, 20% is a suitable concentration and can be adjusted if necessary for this study.

Different PEGDA concentrations or the addition of other ingredients (e.g., cells, growth factors) may affect the curing time and droplet diameter. In future work, the effects of different material concentrations on printing parameters will be considered. Cells will be added to the material for in-situ printing on the basis of this feasibility study.

5. Conclusions

In this paper, a potential in-situ printing platform was built using a small-scale robotic arm equipped with a double-light-source nozzle system. Robotic arm, light source and nozzle were coordinately controlled by a computer interface where the droplet diameter, curing time, and mechanical properties were measured and printing parameters (e.g., nozzle velocity, nozzle frequency) were determined. The feasibility study of in-situ printing on a curved surface was performed on the defect model. In-situ repairing was successfully conducted using both parallel and ring printing paths. The experimental results show that the robotic arm has the capability to achieve hydrogel printing and the liquid material could cure rapidly on the curved surface. The platform is expected to be used for actual in-situ printing in the future.

Supplementary Materials: Supplementary materials are available online at <http://www.mdpi.com/2076-3417/7/1/73/s1>.

Acknowledgments: This work was supported by grants from the Native Science Foundation of China (No. 51375371 and 51323007), the National High Technology Research and Development Program of China (No. 2015AA020303).

Author Contributions: Xiao Li performed the experiments and analyzed the data; Qin Lian and Hua Xin guided the writing of the article and made some modifications; Qin Lian, Dichen Li and Shuhai Jia gave some constructive suggestions; Xiao Li and Hua Xin wrote the paper.

Conflicts of Interest: The authors declare no conflicts of interest.

References

1. Chen, D.; Liu, Y.; He, J.; Wang, Z.; Jin, Z. Research Status and Future of In-Situ Three-Dimensional Printing Technique. *Chin. J. Reparative Reconstr. Surg.* **2014**, *28*, 1428–1430.
2. Ozbolat, I.T. Bioprinting Scale-Up Tissue and Organ Constructs for Transplantation. *Trends Biotechnol.* **2015**, *33*, 395–400. [[CrossRef](#)] [[PubMed](#)]
3. Binder, K.W. In-Situ Bioprinting of the Skin. Ph.D. Thesis, Wake Forest University, Winston-Salem, NC, USA, 2011.
4. Cui, X.; Breitenkamp, K.; Finn, M.G.; Lotz, M.; D’Lima, D.D. Direct Human Cartilage Repair Using Three-Dimensional Bioprinting Technology. *Tissue Eng. A* **2012**, *18*, 1304–1312. [[CrossRef](#)] [[PubMed](#)]
5. Yan, S.F.; Zhang, X.; Zhang, K.X.; Di, H.; Feng, L.; Li, G.F.; Fang, J.J.; Cui, L.; Chen, X.S.; Yin, J.B. Injectable In-situ Forming Poly(L-glutamic acid) Hydrogels for Cartilage Tissue Engineering. *J. Mater. Chem. B* **2015**, *4*, 947–961. [[CrossRef](#)]
6. Uttayarat, P.; Boonsirichai, K.; Tangthong, T.; Pimton, P.; Thongbopit, S.; Phermthai, T. Photopolymerization of Hydrogels for Cartilage Tissue Engineering. In Proceedings of the IEEE Biomedical Engineering International Conference, Pattaya, Thailand, 25–27 November 2015.
7. Devalla, V.; Island, U.O.R. da Vinci Surgical Systems. *Biomed. Saf. Stand.* **2012**, *42*, 84.
8. Mogas-Soldevila, L.; Duro-Royo, J.; Oxman, N. Water-based Robotic Fabrication: Large-Scale Additive Manufacturing of Functionally-Graded Hydrogel Composites via Multi-Chamber Extrusion. *3D Print. Addit. Manuf.* **2014**, *1*, 141–151. [[CrossRef](#)]

9. Lee, W.; Debasitis, J.C.; Lee, V.K.; Lee, J.H.; Fischer, K.; Edminster, K.; Park, J.C.; Yoo, S.S. Multi-Layered Culture of Human Skin Fibroblasts and Keratinocytes through Three-Dimensional Freeform Fabrication. *Biomaterials* **2009**, *30*, 1587–1595. [[CrossRef](#)] [[PubMed](#)]
10. Dababneh, A.B.; Ozbolat, I.T. Bioprinting Technology: A Current State-of-the-Art Review. *J. Manuf. Sci. Eng.* **2014**, *136*, 061016. [[CrossRef](#)]
11. Mandrycky, C.; Wang, Z.; Kim, K.; Kim, D.H. 3D Bioprinting for Engineering Complex Tissues. *Biotechnol. Adv.* **2016**, *34*, 422–434. [[CrossRef](#)] [[PubMed](#)]
12. Bertassoni, L.E.; Cecconi, M.; Manoharan, V.; Nikkhah, M.; Hjortnaes, J.; Cristino, A.L.; Barabaschi, G.; Demarchi, D.; Dokmeci, M.R.; Yang, Y. Hydrogel Bioprinted Microchannel Networks for Vascularization of Tissue Engineering Constructs. *Lab Chip* **2014**, *14*, 2202–2211. [[CrossRef](#)] [[PubMed](#)]
13. Li, Z.C.; Lian, Q.; Jia, S.H.; Lv, Y.; Li, D.C. Study on the Process of the Ink Jet Printing for Photo-curable Hydrogel. *Electromach. Mould* **2015**, *5*, 38–42.
14. Hockaday, L.A.; Kang, K.H.; Colangelo, N.W.; Cheung, P.Y.; Duan, B.; Malone, E.; Wu, J.; Girardi, L.N.; Bonassar, L.J.; Lipson, H.; et al. Rapid 3D Printing of Anatomically Accurate and Mechanically Heterogeneous aortic Valve Hydrogel Scaffolds. *Biofabrication* **2012**, *4*, 035005. [[CrossRef](#)] [[PubMed](#)]
15. Pereira, R.F.; Bártolo, P.J. 3D Bioprinting of Photocrosslinkable Hydrogel Constructs. *J. Appl. Polym. Sci.* **2015**, *132*, 42458. [[CrossRef](#)]
16. Billiet, T.; Gevaert, E.; Schryver, T.D.; Cornelissen, M.; Dubruel, P. The 3D Printing of Gelatin Methacrylamide Cell-laden Tissue-engineered Constructs with High Cell Viability. *Biomaterials* **2013**, *35*, 49–62. [[CrossRef](#)] [[PubMed](#)]
17. Zhu, L.Z.; Lian, Q.; Jin, Z.M.; Li, D.C. Fabrication and Evaluation of PEGDA Hydrogel by Stereo-lithography for Cartilage Tissue Engineering. *J. Xi'an Jiaotong Univ.* **2012**, *46*, 121–126.
18. Kang, K.H.; Hockaday, L.A.; Butcher, J.T. Quantitative Optimization of Solid Freeform Deposition of Aqueous Hydrogels. *Biofabrication* **2013**, *5*, 035001. [[CrossRef](#)] [[PubMed](#)]
19. Turturro, M.V.; Sokic, S.; Larson, J.C.; Papavasiliou, G. Effective Tuning of Ligand Incorporation and Mechanical Properties in Visible Light Photopolymerized Poly(ethylene glycol) Diacrylate Hydrogels Dictates Cell Adhesion and Proliferation. *Biomed. Mater.* **2013**, *8*, 25001–25012. [[CrossRef](#)] [[PubMed](#)]



© 2017 by the authors; licensee MDPI, Basel, Switzerland. This article is an open access article distributed under the terms and conditions of the Creative Commons Attribution (CC-BY) license (<http://creativecommons.org/licenses/by/4.0/>).